Macromolecules **2002,** *35,* 9813−9818

Direct Observation of Crystal−Amorphous Interphase in Lamellar Semicrystalline Poly(ethylene terephthalate)

D. A. Ivanov,[†] T. Pop,[‡] D. Y. Yoon,[*,§] and A. M. Jonas[⊥]

Laboratoire de Physique des Polymères, CP 223, Université Libre de Bruxelles,
B-1050 Brussels, Belgium; Physics Department, "Politehnica" University of Bucharest,
Bucharest, Romania; School of Chemistry, Seoul National University, Seoul 151-747, Korea; and
Unité de physique et de chimie des hauts polymères, Université catholique de Louvain,
B-1348 Louvain-la-Neuve, Belgium

Received October 15, 2001; Revised Manuscript Received August 22, 2002

ABSTRACT: We report on the direct evidence in real space of the crystal−amorphous interphase in a lamellar semicrystalline polymer, poly(ethylene terephthalate) (PET). This evidence was obtained by the TEM observation of the compositional variation of (stained) PET segments in the boundary of an isolated lamellar stack in a binary blend of semicrystalline PET with amorphous poly(ether imide). The lamellar morphology exhibited by the TEM image of a stained lamellar stack was also investigated in detail, in terms of the thickness distributions of lamellar crystallites and noncrystalline interlamellar layers. The validity of employing our TEM imaging method through differential staining of PET segments was then ascertained by comparing the power spectral density obtained from the TEM data with the measured small-angle X-ray scattering profile from semicrystalline PET samples. Compared with this lamellar morphology, the thickness of the observed crystal−amorphous interphase at the boundary of the lamellar crystallites and (mixed) random melts is even greater than the thickness of the noncrystalline interlamellar layer of PET. This striking result may be attributed to the rigid aromatic groups in the PET chain backbone which prohibit the occurrence of tight chain folding. Accordingly, the entire noncrystalline interlamellar region of aromatic semicrystalline polymers may be regarded as the interphase, devoid of truly random amorphous phase.

Introduction

The microstructure of polymer molecules within the noncrystalline region of a semicrystalline morphology and the nature of the crystal−amorphous boundary are central to understanding the important physical properties of semicrystalline polymers. However, the extreme complexity of polymer organization on various length scales has turned this topic into a very controversial and highly debated issue for about four decades.[1] Many experimental and theoretical studies dedicated to this subject were undertaken during this time. For example, important information on the molecular morphology of semicrystalline polymers can be obtained from neutron scattering experiments carried out on mixtures of hydrogeneous and deuterated polymers. In particular, the examination of the scattering patterns at low angles (small-angle neutron scattering) allows one to determine the radius of gyration (R_g) of polymer chains. For polymers crystallized from dilute solutions, R_g is found to decrease significantly upon crystallization. In contrast, experiments for a diverse set of polymers, such as polyethylene (PE),[2,3] isotactic polypropylene,[4,5] and poly(ethylene terephthalate) (PET),[6] show that R_g does not change upon crystallization from the melts. This finding is not reconcilable with the classical model of regularly chain-folded polymer crystals with adjacent reentry of the crystalline stems.[2] The local placements of crystalline stems belonging to the same polymer chain were further investigated by modeling the intermediate-angle neutron scattering profiles.[6,7] These analyses provide strong indications that arrays of nearest-neighbor reentries (tight folds) are not the major occurrence for melt-crystallized polymers. However, the neutron scattering results do not provide detailed information on the chain trajectories in the noncrystalline regions.

The existence of interfacial regions whose properties would be intermediate between those of crystalline and amorphous regions has been shown by quantitative comparisons of the degree of crystallinity as determined by different methods, such as density, X-ray diffraction, DSC, and Raman or infrared spectroscopy.[1,8−11] Moreover, small-angle X-ray scattering (SAXS) experiments also provide hints to the existence of density transition layers at crystalline lamellar surfaces. In this context, nuclear magnetic resonance (NMR) is a very powerful tool to identify interfacial regions based on the differences in chemical shift patterns and relaxation properties. Early on, the complex appearance of the proton broad line NMR spectra of linear PE comprising three components of varying mobility has been interpreted as a manifestation of the deficiency of the two-phase model for a semicrystalline polymer. Detailed measurements of spin−spin relaxation[12,13] and spin diffusion[14] by ^{1}H and/or ^{13}C NMR have confirmed the existence of transition regions at crystal boundaries. In addition, solid-state high-resolution ^{13}C NMR spectra of melt-crystallized polyethylene samples show a separate chemical shift attributed to the crystal−amorphous interphase.[12]

Complementary information concerning the chain structure in the noncrystalline regions in semicrystalline polymers has also been provided by the experimental results on the dynamics and mobility of noncrystalline chain segments, obtained from differential scanning

---

[†] Université Libre de Bruxelles.
[‡] "Politehnica" University of Bucharest.
[§] Seoul National University.
[⊥] Université catholique de Louvain.
[*] To whom correspondence should be addressed.

10.1021/ma011784j CCC: $22.00

calorimetry (DSC), dynamic mechanical thermal analysis (DMTA), and dielectric relaxation analysis. In particular, these techniques allow the determination of changes in the glass transition temperature (T_g) and the parameters of the associated relaxation (e.g., the corresponding relaxation strength) upon crystallization. A large number of experimental data acquired on the relaxation properties of semicrystalline polymers are analyzed in a recent review[15] mainly focusing on the family of aromatic polyesters and polyamides. For this group of polymers, it has been found that the glass transition temperature increases and the corresponding normalized relaxation strength decreases upon crystallization. In particular, the dramatic reduction of the normalized relaxation strength has brought about the concept of a "rigid amorphous fraction".[16] This fraction of noncrystalline material, which is unable to exhibit the relaxational characteristics of liquidlike amorphous regions and thus does not contribute to the change in the dielectric permittivity and the specific heat, was later attributed to the crystal−amorphous interphase.[17] In this regard, such a decrease of the relaxation strength has been generally observed for various semicrystalline polymers ranging from poly(ether ether ketone) to polyesters, polyamides, and polyimides.

Despite the fact that the existence of the interphase in semicrystalline polymers seems thus to be thoroughly demonstrated, serious discrepancies among authors remain with respect to the quantitative characterization of this interphase. Indeed, depending on the property probed by a given experimental technique, different results will be obtained, leading to a technique-dependent definition of crystal/amorphous boundaries. Moreover, the determination of the interfacial dimensions by scattering or spin-diffusion measurements invariably depends on complex modeling and thus lacks an independent direct information on the interfacial microstructure.

In contrast, a more specific definition of the crystal−amorphous interphase, which is the region of partial order in the semicrystalline structure, can be provided from the computations based on lattice calculations using the Bragg−Williams mean-field approximation[18−23] or off-lattice Monte Carlo simulations.[24,25] The results can be summarized as follows: According to the lattice model, the structure of the interphase strongly depends on the tight-fold energy, E_η, a parameter introduced to account for the energy expenditure required to form a tight fold. The interphase thickness increases with the value of E_η. For large E_η values, the order can persist over several lattice layers away from the crystal surface. However, considerable uncertainty can be introduced in these calculations via the choice of the model parametrization. In addition, the lattice is considered to be completely filled, so the effect of a density change in the amorphous region[26] is not included in these calculations. These shortcomings have been improved in the off-lattice Monte Carlo simulations[24,25] performed employing a freely rotating chain model and a series of moves designed to equilibrate the conformational and topological spaces. In particular, Monte Carlo simulation study of the effect of the tilt angle between crystalline stems and lamellar normal on the chain conformations in the crystal−amorphous interphase revealed a dramatic decrease of the number of tight folds as this tilt angle increases.[25]

Therefore, although the very existence of the order−disorder transition region at the crystal−amorphous boundaries in melt-crystallized lamellar semicrystalline polymers is well established, there is a serious lack of *direct experimental* demonstration of this crystal−amorphous interphase. A direct visualization of the interphase necessarily requires a way to identify regions according to their local order, with a spatial resolution on the scale of the nanometer. The situation is made worse by the fact that real semicrystalline polymer systems typically display a complex hierarchical microstructure consisting of stacks of locally parallel lamellae organized on a larger scale into entities with a spherical symmetry, i.e., spherulites.

In the present work, to surmount these difficulties, we have employed a special double-marking procedure that allows the observation of the interphase by transmission electron microscopy (TEM). The first marking is performed by adding probe molecules which, through the solubility characteristics, demark the local thermodynamic environment in the semicrystalline polymer, i.e., the chemical potential, which varies with the local order. The second marking is then realized through the preferential staining of such internally marked samples which varies with the local composition and the diffusivity of stain agents.

For the probe molecules of the first marking, we employed a noncrystallizable polymer which is fully miscible with the semicrystalline polymer in the amorphous melts. At first sight, this blending introduces additional complexity into the system, since the crystallizable component (component A) will tend to reject the noncrystallizable polymer (B) from the growing crystals during crystallization. Therefore, a complex segregation behavior of B is expected, as suggested by Keith and Padden,[27] depending upon the crystal growth rate and the rate of mutual diffusion. On the other hand, the B component has the capability to act as a probe capable of assessing the local order, or local chemical potential, of the A segments emanating from the lamellar crystallites into the crystal−amorphous interphase. That is, this local variation in chemical potential of the A segments in the crystal−amorphous interphase should be reflected by the miscibility with the B segments and thus be manifested by a local variation of the concentration of B segments in the vicinity of lamellar crystallites of A polymer. Keeping in mind that the free energy balance upon mixing a pair of not-too-strongly interacting polymers is very fragile, one can expect that the partial ordering of the A segments at the lamellar boundaries will significantly modify the corresponding miscibility characteristics with polymer B.

In fact, this situation was investigated theoretically in refs 22 and 23, which extended the lattice calculations of the crystal−amorphous interphase of pure semicrystalline polymers to the binary blends of semicrystalline and amorphous polymers which are completely miscible in the amorphous melts. The theoretical calculations, performed for the boundary region between the lamellar surface of semicrystalline polymer A and the mixed equilibrium melts of A and B polymers, indeed show that for moderately interacting polymers (interaction parameter χ_{AB} not strongly negative) the solubility or the concentration profile of noncrystallizable polymer component B is strongly affected by the degree of order in the interphase of semicrystalline polymer A. This means that a compositional interphase appears in the noncrystalline regions in the immediate vicinity of the lamellar crystallite of polymer A, which is in contact with the mixed amorphous melts of A and B polymers. Moreover, the degree of order in the interphase is hardly affected by the presence of the noncrytallizable polymer B. This is because the free energy expenditure associated with the mixing of A and B segments is negligible when compared to the other factor associated with the dissipation of order.[23] Therefore, the width of the compositional interphase may represent a good estimate of the crystal–amorphous interphase of lamellar semicrystalline polymers

Experimental Section

To experimentally visualize the compositional interphase, we have selected a pair of polymers, semicrystalline PET and amorphous poly(ether imide) (PEI), which are well-known to be fully miscible in the amorphous state.[28] PET was obtained from ICI (grade E47; $M_n = 19\,000$ and $M_w = 42\,000$ as determined by size exclusion chromatography in a 98/2 by volume chloroform/hexafluoro-2-propanol mixture, using universal calibration). PEI was received from General Electric (grade ULTEM 1000; $M_n = 25\,400$ and $M_w = 70\,320$ as determined by size exclusion chromatography in a 98/2 by volume chloroform/hexafluoro-2-propanol mixture, using a calibration curve based on PMMA standards). Blends were prepared in solutions by separately dissolving PET and PEI in a mixture of phenol and tetrachloroethane (50/50 by weight) and mixing the solutions at room temperature. The solutions were then cast on glass slides, the solvents evaporated at elevated temperature (413 K, 1 min), and the films quenched into water to get fully amorphous films (ca. 10–20 μm thick). These films were floated off onto Milli-Q water and dried under vacuum overnight. This choice of solution blending procedure over the melt blending was made in order to prevent the chemical reaction between PET and PEI which occurs rapidly during the melt blending which has to be performed at high temperatures.[29] The existence of this chemical reaction was completely overlooked in the previous studies on these blends.[30] The films were subsequently crystallized from the glassy state at the desired temperatures for 9.5 h under argon.

For transmission electron microscopy (TEM) studies, the thin films of PET/PEI were embedded in epoxide resin, trimmed with a razor blade to the shape of truncated pyramids, and microtomed using a Reichert UCT apparatus fitted with a diamond knife. Ultrathin sections (approximately 50–100 nm thick) of the samples supported on 400 mesh TEM grids were subsequently exposed to the vapors of the ruthenium trichloride hydrate/sodium hypochlorite mixture in accordance with the procedure described elsewhere.[31] Stained sections were observed with a Philips EM 301 transmission electron microscope operating at 80 kV. The photograph was scanned and then imported into a homemade analysis program running under Wavemetrics Igor Pro. The image was flattened by subtracting line-by-line polynomials of second-order fit to the gray level background outside the lamellar stack.

Small-angle X-ray scattering (SAXS) experiments were performed with an evacuated Kratky compact camera mounted on a Siemens rotating anode generator (Ni-filtered Cu Kα radiation, 40 kV/300 mA). A position-sensitive proportional counter (PSPC, Braun) was used to record the scattering patterns. The raw data were corrected for absorption, parasitic scattering, detector dead time, and the fluidlike background in accordance with ref 10. The diffraction curves were finally desmeared with a variant of Glatter's algorithm[32] and multiplied by a Lorentz factor s^2, with $s = 2\sin(\theta/2)/\lambda$ where θ is the angle between incident and scattered beams and λ is the X-ray wavelength. The selected Lorentz factor (s^2) corresponds to the lamellar geometry of scatterers.

Image Processing

A complete account of the processing of TEM images of semicrystalline polymers will be reported elsewhere.[33] Briefly, the TEM negative was scanned using a calibrated high-resolution scanner to produce a 2D matrix of gray levels, $h(x,y)$. For the oriented stack studied in this paper, x was taken in the direction parallel to the stack, and y was perpendicular to the stack (see Figure 1). Distributions of thickness for amorphous and crystalline regions were simply obtained by measuring the distances between successive boundaries in the lamellar stack over a series of lines drawn perpendicular to the lamellar stack. For the lamellar stack of Figure 1, 411 such lines were drawn at a distance of 1.3 nm from each other in the central part of the lamellar stack (excluding stack ends where either lamellae diverge or contrast is insufficient). Crystal boundaries were defined as the location corresponding to the average gray value between the gray values of two successive maxima and minima. The distances were computed over a region going from the center of the first lamella to the center of the last lamella, effectively excluding transition regions between the free melt and the bordering lamellae from our computations. To eliminate spurious errors due to the automated treatment, 5% of the extremely low and high values were rejected from the distributions. This rejection procedure does not affect significantly the average values but eliminates unrealistic low and high distance tails in the distributions. Alternative ways to obtain size distributions based on thresh holding followed by successive erosion and dilation operations[34] were not performed here.

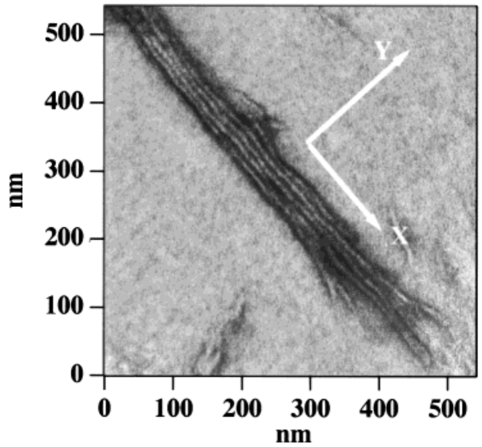

Figure 1. Flattened TEM image of a lamellar stack grown in a PET/PEI 20/80 blend crystallized for 9.5 h at 473 K. The microtomed section was exposed to vapors of a ruthenium trichloride hydrate/sodium hypochlorite solution, which stains the noncrystalline PET segments to appear dark in the micrograph.

Image processing was also performed in reciprocal space by first computing a normalized 2D power spectral density, $P_2(s_x,s_y)$. P_2 was computed on the image stripped of the tips of the stack after multiplication by a Welch function to eliminate Fourier ripples:[35]

$$P_2(s_x,s_y) = \frac{1}{S}\left|\int_S h(x,y)\, W(x,y)\, e^{2\pi j(s_x x + s_y y)}\, dx\, dy\right|^2$$

where S is the surface of the image and W the Welch function. Next, a one-dimensional power spectral density $P_1(s)$ was obtained in the direction perpendicular to the stack:

$$P_1(s) = P_2(0,s_y{=}s)$$

For the aligned stack studied in the present paper, $P_1(s)$ is the optical equivalent of the SAXS intensity that would be measured for scattering vectors perpendicular to the stack. Hence, the standard techniques developed for the SAXS intensity analysis can be directly applied to $P_1(s)$.

Results and Discussion

The solid-state microstructure of the amorphous PET/PEI blends was found to be homogeneous, as each blend exhibits only a single glass transition temperature (T_g) which can be well approximated by the Fox–Flory relationship. No indications were found for the presence of an upper critical solution temperature (UCST) as reported by others.[30] Instead, we observed a liquid–liquid phase separation at high temperatures, with a lower critical solution temperature, LCST, of about 538 K (blend 50/50). The annealing of amorphous blends from the glass at temperatures between 433 and 493 K resulted in semicrystalline samples employed in the study.

The preliminary characterization of the semicrystalline blends was presented in ref 29, and the detailed description will be presented separately. Here, we focus on the TEM results obtained on PEI-rich blends crystallized at relatively high temperatures (at and above 473 K), which are the most interesting ones with respect to our objective of direct visualization of the crystal–amorphous interphase. A TEM picture of a stained microtomed section of PET/PEI 20/80 crystallized for 9.5 h at 473 K is displayed in Figure 1. For such a PET dilute blend at 473 K, the crystallization is very slow and does not reach vitrification even after 9.5 h of annealing. (Vitrification can occur in miscible binary semicrystalline–amorphous blends on isothermal annealing within the temperature window located between the T_g of the blend and the T_g of its pure amorphous component.[36]) It produces an incompletely space-filling structure consisting of small immature spherulites or sheafs[37] (not shown here). These conditions are therefore ideal to allow isolated lamellar stacks to be observed in great detail. As was checked in prior experiments, the stain reaction selectively marks amorphous PET, leaving PEI practically untouched. In addition, because the diffusivity of the stain in PET crystals is much slower than that in amorphous regions, PET crystals appear as gray stripes in the micrographs. The noncrystalline matrix surrounding the lamellar stack remains practically unstained, since it is very PEI-rich (more than 80 wt %).

Of particular importance here is the presence of two black stripes bordering the stack, which directly signals the existence of PEI-depleted regions at the surfaces of the first and last PET lamellae which are neighboring the mixed amorphous melts. The existence of such PEI-depleted noncrystalline PET regions is in accordance with the compositional interphase predicted by theory as discussed above. However, to carry out a detailed, quantitative characterization of this interphase, one needs to check out whether the lamellar structure as observed by the TEM imaging of the PET–PEI blend specimen is consistent with the lamellar semicrystalline morphology of the bulk PET sample.

Figure 1 also shows that PET lamellae are separated by PET-rich amorphous regions, which indicates only restricted PEI interlamellar inclusion, if any. This is consistent with observations by other techniques (SAXS and DMTA) for the samples prepared under identical conditions with high PET contents.[29] For quantitative characterization, we have employed image analysis techniques to study the lamellar semicrystalline structure shown in Figure 1. Distributions of the thickness for crystalline lamellae, noncrystalline interlayers, and long periods (i.e., the repeat period of the lamellar stacking) thus obtained are presented in Figure 2. Number-average values are 5.3 nm for the crystal thickness, 6.2 nm for the noncrystalline interlayer thickness, and 10.5 nm for the long period. The asymmetry of distributions results in the average long period being smaller than the sum of the average thickness of crystalline and noncrystalline layers. It is important to note the relatively large standard deviations of the thickness distributions (1.5 nm for the crystal thickness, 2.0 nm for the noncrystalline interlayers, and 2.9 nm for the long period) even for this simple system (single stack). It is thus not surprising that extracting average crystal thickness by applying simple models to interpret the SAXS data for semicrystalline polymers is prone to large uncertainties.[38]

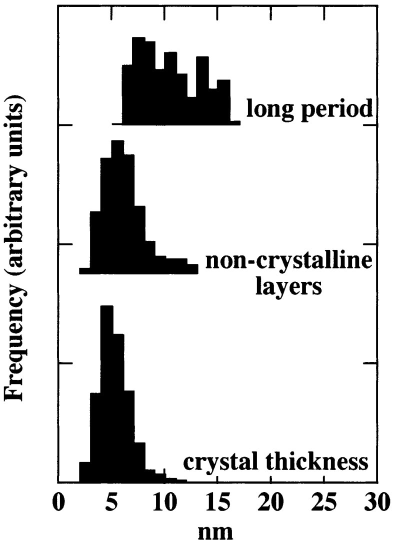

Figure 2. Distributions of thickness for the long period, the noncrystalline interlayers and the lamellar crystal thickness, as determined from the lamellar stack of Figure 1.

The results obtained by the direct analysis of the TEM image can be checked by performing other measurements. We thus computed the 2D power spectral density of the image (i.e., its optical transform), $P_2(s)$. Figure 3 (curve a) reports the variation of this spectral density along a vector passing through the origin of reciprocal space, drawn perpendicular to the lamellar stack (i.e., in the *Y* direction with respect to the notation in Figure 1). This one-dimensional PSD, $P_1(s)$, shows first a rapidly oscillating decrease with reciprocal length, corresponding to the form factor of the stack (a $\sin^2(q)/q^2$ function). Accordingly, this portion of $P_1(s)$ can be mostly suppressed by setting gray values of the background surrounding the stack to the average gray level of the stack, as shown in Figure 3 (curve b). The remaining part of $P_1(s)$ essentially consists of a broad peak located at about 0.09 nm^{-1}, due to the internal structure of the stack, the position of which is virtually insensitive to the gray level of the surroundings of the stack (compare curves a and b in Figure 3). The main broad peak is superimposed by a series of oscillations resulting from its convolution by the form factor of the stack. This main peak detected in $P_1(s)$ is similar in nature to the small-

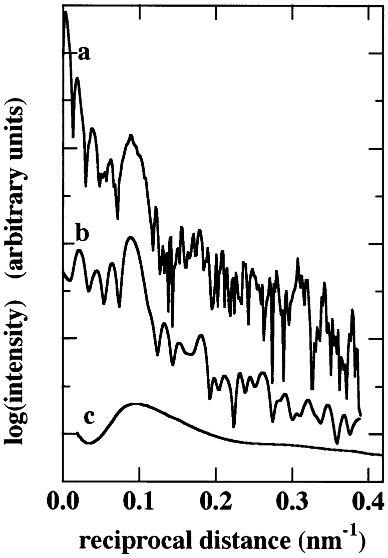

Figure 3. (a) One-dimensional power spectral density of Figure 1 along a line passing through the origin of reciprocal space and drawn perpendicular to the stack (*Y* direction of Figure 1). This curve displays central oscillations due to the form factor of the stack and a broad peak at about 0.09 nm^{-1} resulting from the repeat pattern inside the stack. (b) The same 1D PSD computed on an image where pixels of the amorphous background have been set to the average value of gray level inside the stack. (c) Lorentz-corrected desmeared small-angle X-ray scattering profile for a bulk PET sample crystallized under a condition identical to that employed for the PET−PEI blend of Figure 1.

angle X-ray scattering peak usually observed for semicrystalline polymers, though the latter originates from the spatial correlations of the electron density rather than the photographic density as is the case for $P_1(s)$. The maximum of the main broad peak of $P_1(s)$ corresponds to a long period of 11.1 nm, which is in good agreement with 10.5 nm determined in direct space, confirming the validity of our evaluations.

It is important to compare $P_1(s)$ of the stack to the SAXS pattern obtained on *bulk* PET crystallized under the identical conditions (Figure 3, curve c). The long period of pure PET crystallized for 9.5 h at 473 K amounts to 10.5 nm, which compares well with the 10.5−11.1 nm (direct and reciprocal space analyses, respectively) determined by TEM on the PET/PEI 20/80 blend. Considering that our previous SAXS study showed that the presence of PEI does not perceptively modify the semicrystalline organization of PET at the lamellar scale,[29] this good agreement between the SAXS and the TEM results demonstrates the validity of our TEM imaging method.

By the way, the SAXS peak for the pure PET sample appears significantly broader than the corresponding peak in the 1D PSD of the blend. This indicates substantially higher disorder of the lamellar packing in bulk PET as compared with the single lamellar stack examined by TEM. This is not surprising, given the width of the distributions already discussed for the isolated stack. Indeed, one must conclude that such distributions are very broad for the bulk PET sample, which again implies that simple interpretations of the SAXS data from semicrystalline PET, without due considerations of broad distributions of the thickness of crystalline and noncrystalline layers as commonly found in the literature, are likely to be subject to large uncertainties.

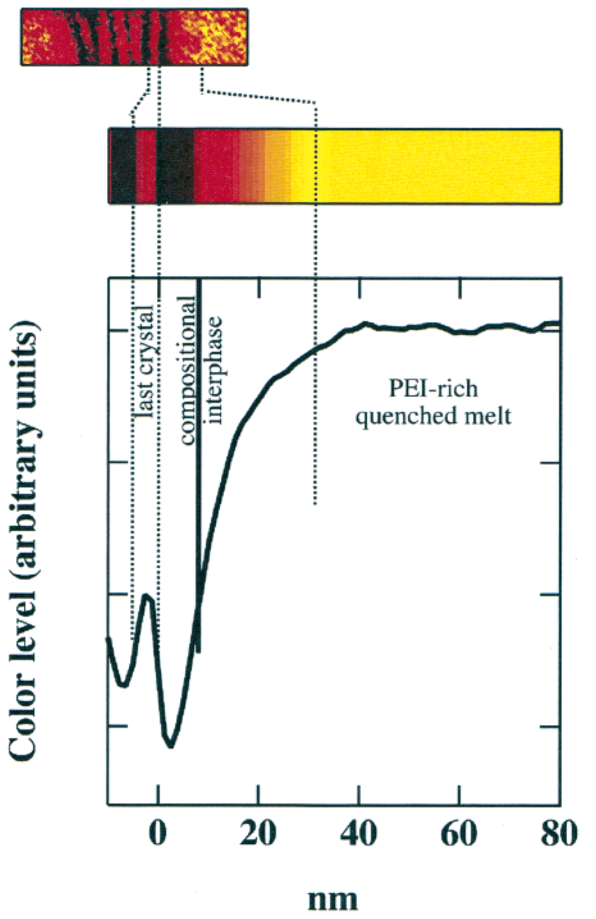

Figure 4. Average darkening level as a function of distance from the boundary of the last (or first) lamella of the stack (color code: black indicates strongly stained regions; red indicates moderately stained regions; yellow indicates slightly stained regions). The interface of the last lamella is located at zero (see text). The variation of gray level from this interface toward the free PEI-rich quenched melt is roughly proportional to PEI concentration.

Finally, we can now return to the PEI concentration profile at the interface between the last (or the first) PET lamella and the PET/PEI quenched melt. We present in Figure 4 the average variation of film darkening from the boundary of the outer crystal toward the quenched random melt and its color image with the following color code: black indicates strongly stained regions, red indicates moderately stained regions, and yellow indicates slightly stained regions. The crystal boundary, which is set to position zero, is defined as the location where the darkening level is halfway between the minimum darkening level in the last (or first) lamella of the stack and the maximum darkening level in the PEI-depleted layer bordering the stack. Averaging was performed while shifting each independent local profile so as to match the location of the crystal boundary in each profile, allowing to reduce broadening of the average profile due to stack waviness. The profile was obtained by averaging over 312 lines drawn perpendicular to the stack; both left and right interfaces have been included in the averaged profile. Because each profile was shifted in order to bring the crystal interface at location zero before averaging, and due to the relatively large distribution of crystal thickness, the average gray level of the last lamella is lower than that on the original photograph due to smearing. The darkening level in the quenched melt is roughly proportional to the PET content. One observes a significant depletion of PEI near the border of the lamellar stack, with a quasi-exponential return to equilibrium concentration deeper into the quenched melt. As pointed out already, the existence of this PEI depletion layer is clearly seen in Figure 1 through the appearance of the two dark stripes bordering the lamellar stack. The integral width of the depletion layer amounts to 12.4 nm, while the darkening level corresponding to half the value of the background is found at 10.3 nm from the crystal surface. These are considerable distances indeed, comparable to the long period (ca. 11 nm) of the lamellar stack.

This compositional interphase, which is in full agreement with the theoretical prediction, may be taken as a good representation for the order−disorder interphase. Our results thus suggest that the order−disorder transition at the boundary of the lamellar crystallite and the random amorphous melt of PET extends over similarly large distances. Therefore, the surprising conclusion follows that the crystalline order appears to be dissipated at distances greater than the average thickness of the interlamellar noncrystalline layer in semicrystalline PET. This result may arise from the presence of rigid aromatic groups in the PET chain backbone, which will effectively exclude the formation of tight folds in significant amount. Hence, noncrystalline PET segments in the interlamellar region may be devoid of truly random amorphous characteristics.

Conclusions

We have carried out detailed analyses of TEM images of stained semicrystalline PET/PEI blends. The introduction of PEI makes it possible to probe the local order, or chemical potential, in the noncrystalline region between the PET lamellar surface and the mixed random amorphous melts without disturbing the lamellar morphology as compared with the bulk semicrystalline PET. The distributions of thickness for the crystalline and the noncrystalline regions in the lamellar stack are quite broad, even for the quasi-ideal sample of a single stack, thus raising a serious question on the accuracy of the detailed analysis of the small-angle X-ray scattering data from semicrystalline polymers. As the most important finding of this study, we successfully carried out the direct imaging of a compositional interphase at the boundaries of lamellar crystallites and the mixed random melts, which points to the existence of the order−disorder interphase of a size greater than the thickness of interlamellar noncrystalline layers. Consequently, the semicrystalline state of PET should be regarded as being comprised of lamellar crystalline regions separated by noncrystalline regions of partial order. Such considerations are also expected to apply to a variety of other aromatic semicrystalline polymers such as aromatic poly(ether ketone)s and poly(alkene terephthalate)s. Moreover, this finding will be important to understanding various physical properties of PET and other aromatic semicrystalline polymers as well as the formation of lamellar stacks upon crystallization.

Acknowledgment. The authors acknowledge the excellent technical support provided by Ms. P. Lipnik for TEM experiments. The authors thank Ms. Z. Amalou for the help in preparation of PET/PEI blends and the DSC measurements. We also acknowledge support by the Belgian National Fund for Scientific Research. T.P. acknowledges the AUPELF-UREF for a grant of perfection by researching and Catholic University of Louvain-la-Neuve for providing the financial support through the Program of Collaboration with Central and East-European Countries and thanks Prof. J. P. Issi for his continuing interest and support. D.Y.Y. acknowledges the support from the Chemistry and Molecular Engineering Division of the Brain Korea 21 Project.

References and Notes

(1) Mandelkern, L. *Chemtracts: Macromol. Chem.* **1992**, *3*, 347.
(2) Sadler, D. M.; Keller, A. *Macromolecules* **1977**, *10*, 1128.
(3) Flory, P. J. *Pure Appl. Chem.* **1984**, *56*, 1667.
(4) Yoon, D. Y.; Flory, P. J. *Polym. Bull. (Berlin)* **1981**, *4*, 693.
(5) Ballard, D. G. H.; Cheshire, P.; Longman, G. W.; Schelten, J. *Polymer* **1978**, *19*, 379.
(6) Wignall, G. W. In *Physical Properties of Polymers*, 2nd ed; Mark, J. E., Ed.; American Chemical Society: Washington, DC, 1993.
(7) Fischer, E. W.; Hahn, K.; Kugler, J.; Struth, U.; Born, R.; Stamm, M. *J. Polym. Sci., Polym. Phys. Ed.* **1984**, *22*, 1491.
(8) Strobl, G. R.; Hagedorn, W. *J. Polym. Sci., Polym. Phys. Ed.* **1978**, *16*, 1181.
(9) Chalmers, J. M.; Everall, N. J. *Trends Anal. Chem.* **1996**, *15*, 18.
(10) Jonas, A. M.; Ivanov, D. A.; Yoon, D. Y. *Macromolecules* **1998**, *31*, 5352.
(11) Singhal, A.; Fina, L. J. *Polymer* **1996**, *37*, 2335.
(12) Kitamaru, R.; Horii, F.; Murayama, K. *Macromolecules* **1986**, *19*, 636.
(13) Shimizu, Y.; Harashina, Y.; Sugiura, Y.; Matsuo, M. *Macromolecules* **1995**, *28*, 6889.
(14) Eckman, R. R.; Henrichs, P. M.; Peacock, A. T. *Macromolecules* **1997**, *30*, 2474.
(15) Aharoni, S. M. *Polym. Adv. Technol.* **1998**, *9*, 169.
(16) Cheng, S. Z. D.; Cao, M.-Y.; Wunderlich, B. *Macromolecules* **1986**, *19*, 1868.
(17) Huo, P.; Cebe, P. *Macromolecules* **1992**, *25*, 902.
(18) Flory, P. J.; Yoon, D. Y.; Dill, K. A. *Macromolecules* **1984**, *17*, 862.
(19) Kumar, S. K.; Yoon, D. Y. *Macromolecules* **1989**, *22*, 3458.
(20) Marqusee, J. A.; Dill, K. A. *Macromolecules* **1986**, *19*, 2420.
(21) Marqusee, J. A. *Macromolecules* **1989**, *22*, 472.
(22) Kumar, S. K.; Yoon, D. Y. *Macromolecules* **1989**, *22*, 4098.
(23) Kumar, S. K.; Yoon, D. Y. *Macromolecules* **1991**, *24*, 5414.
(24) Balijepalli, S.; Rutledge, G. C. *J. Chem. Phys.* **1998**, *109*, 6523.
(25) Gautam, S.; Balijepalli, S.; Rutledge, G. C. *Macromolecules* **2000**, *33*, 9136.
(26) Frank, F. C. *Faraday Discuss. Chem. Soc.* **1979**, *68*, 7.
(27) Keith, H. D.; Padden, F. J. *J. Appl. Phys.* **1963**, *34*, 2409; *J. Appl. Phys.* **1964**, *35*, 1270; *J. Appl. Phys.* **1964**, *35*, 1286.
(28) Martinez, J. M.; Eguiazabal, J. I.; Nazabal, J. *J. Appl. Polym. Sci.* **1993**, *48*, 935.
(29) Ivanov, D. A.; Pop, T.; Yoon, D. Y.; Jonas, A. M. *Polym. Mater. Sci. Eng.* **1999**, *81*, 335.
(30) Chen, H.-L. *Macromolecules* **1995**, *28*, 2845. Chen, H.-L.; Hwang, J. C.; Chen, C.-C.; Wang, R.-C.; Fang, D.-M.; Tsai, M.-J. *Polymer* **1997**, *38*, 2747. Chen, H.-L.; Hsiao, B. S. *Macromolecules* **1998**, *31*, 6579.
(31) Ivanov, D. A.; Lipnik, P. D. M.; Jonas, A. M. *J. Polym. Sci., Polym. Phys. Ed.* **1997**, *35*, 2565.
(32) Glatter, O. *J. Appl. Crystallogr.* **1974**, *7*, 147.
(33) Gallez, X.; Haubruge, H. G.; Jonas, A. M.; Legras, R.; Nysten, B. Manuscript in preparation.
(34) Pratt, W. K. *Digital Image Processing*, 2nd ed.; Wiley & Sons: New York, 1991.
(35) Press: W. H.; Teukolsky, S. A.; Vetterling, W. T.; Flannery, B. P. *Numerical recipes in C. The art of scientific computing*, 2nd ed.; Cambridge University Press: New York, 1992.
(36) Ivanov, D. A.; Jonas, A. M. *J. Polym. Sci., Part B: Polym. Phys. Ed.* **1998**, *35*, 2565.
(37) Bassett, D. C. *CRC Crit. Rev. Solid State Mater. Sci.* **1984**, *12*, 97 and references therein.
(38) Wang, Z. G.; Hsiao, B. S.; Fu, B. X.; Liu, L.; Yeh, F.; Sauer, B. B.; Chang, H.; Schultz, J. M. *Polymer* **2000**, *41*, 1791. Chen, H.-L. *Macromolecules* **1995**, *28*, 2845. Chen, H.-L.; Hwang, J. C.; Chen, C.-C.; Wang, R.-C.; Fang, D.-M.; Tsai, M.-J. *Polymer* **1997**, *38*, 2747. Chen, H.-L.; Hsiao, B. S. *Macromolecules* **1998**, *31*, 6579.

MA011784J